AeroDeeP 2.2
Theory Guide

January 2021

PRINCIPIA

ifP Energies nouvelles

Table of Contents

- vi -

1 Models for HAWTs

1.1 Blade Element Momentum (BEM)

The Blade Element Momentum theory is the most frequently used theory to predict performances of Horizontal Axis Wind Turbines (HAWT) and to predict loads applied on blades ([1], [2], [3]). The goal of this theory is to identify loads applied by a steady-homogeneous-incompressible flow (Mach ≤ 0.3) on a disk representing the area swept by the rotor of a wind turbine (Momentum theory). In parallel to this, power recovered by the wind-turbine rotor according to the wind velocity at the rotor is calculated (Blade Element theory). Finally, an iterative calculation is done until the force applied by the wind on the disc corresponds to the force recovered by the rotor.

1.2 Momentum theory

1.2.1 One-dimensional momentum theory

A stream tube whose section is equal to the section of the rotor at the rotor location is assumed. The flow being assumed incompressible, the velocity and the section are directly proportional. The wind kinetic energy is recovered by the rotor, therefore the wind velocity is lower downstream of the turbine. Thus, this stream tube (Figure 1) has a smaller section than the rotor section in the upstream region (i.e. a higher velocity) and a larger section than the rotor section in the downstream zone (i.e. a lower velocity).
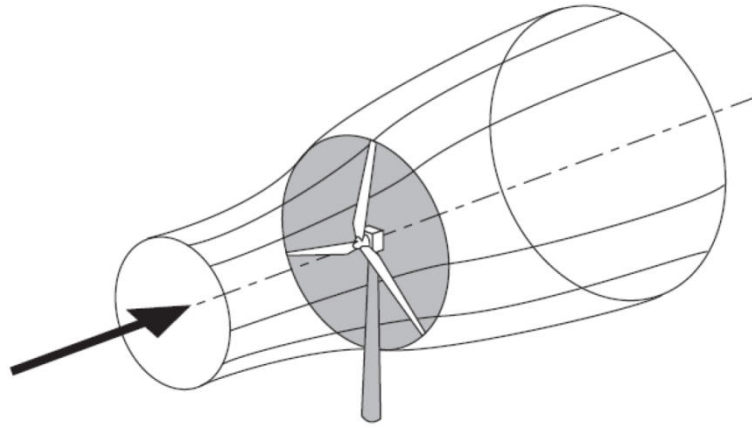
Figure 1: Trajectory of an air particle passing through the rotor disc [4]

A stream tube with pressures and velocities described in Figure 2 is assumed. If T is the thrust force, we can write:

$$T = m(U_\infty - U_w). \tag{1}$$

Using the mass flow rate, m ($m = \rho A U$), we can rewrite the above equation as:

$$T = U_\infty(\rho A U)_\infty - U_w(\rho A U)_w, \tag{2}$$

where ρ and A are respectively the fluid density and the disk section.

Applying the Bernoulli law upstream and downstream of the disk, one obtains the following relationships:

$$\begin{cases} P_\infty + \frac{1}{2}\rho U_\infty^2 = P_D^+ + \frac{1}{2}\rho U_D^2 \\ P_D^- + \frac{1}{2}\rho U_D^2 = P_\infty + \frac{1}{2}\rho U_w^2. \end{cases} \tag{3}$$

The thrust force can be obtained with the pressures on each side of the disk by:

$$T = A(P_D^+ - P_D^-). \tag{4}$$

Consequently, using the Bernoulli law, we can write:

$$T = \frac{1}{2}\rho A(U_\infty^2 - U_w^2). \tag{5}$$
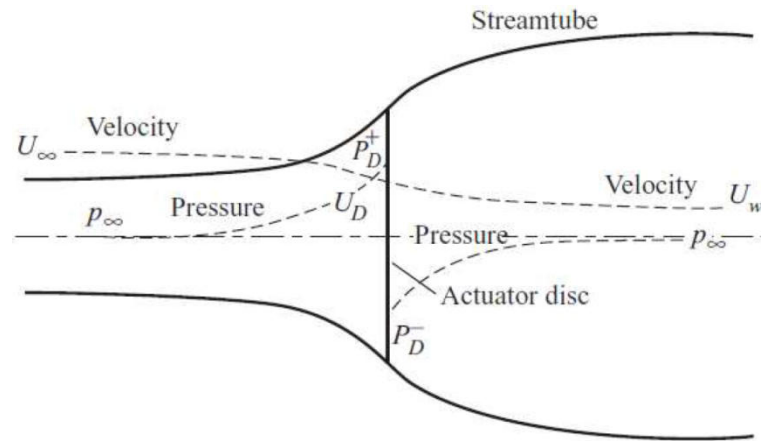
Figure 2: An energy extracting actuator disc and stream-tube [4]

Using Equation 1, the mass flow rate written at the actuator disk $(m = (\rho A U)_D)$, and Equation 5, one obtains an expression for the wind velocity U_D on the actuator disk:

$$U_D = \frac{U_\infty + U_w}{2}. \tag{6}$$

The induction factor a is introduced as:

$$a = \frac{U_\infty - U_D}{U_\infty}. \tag{7}$$

Using this new parameter, U_D and U_w are written as a function of U_∞:

$$\begin{cases} U_D = U_\infty(1-a) \\ U_w = U_\infty(1-2a). \end{cases} \tag{8}$$

Power $(P = U_D T)$ and thrust on the rotor disk can now be written as:

$$\begin{cases} T = \frac{1}{2}\rho A U_\infty^2 4a(1-a) \\ P = \frac{1}{2}\rho A U_\infty^3 4a(1-a)^2. \end{cases} \tag{9}$$

The power and thrust coefficients, C_P and C_T , are defined as the ratio between the power (or thrust) recovered by the rotor and the maximum power (or thrust) that is available in the wind:

$$\begin{cases} C_T = \dfrac{\text{Thrust force}}{\text{Dynamic force}} = \dfrac{T}{\frac{1}{2}\rho A U_\infty^2} = 4a(1-a) \\[3mm] C_P = \dfrac{\text{Rotor power}}{\text{Power in the wind}} = \dfrac{P}{\frac{1}{2}\rho A U_\infty^3} = 4a(1-a)^2. \end{cases} \tag{10}$$

The variation of power and thrust coefficients with the induction factor is shown in Figure 3. One can see that the rotor can recover all the available force of the wind ($C_T = 1$) but not all the power available of the wind ($C_P \approx 0.6$).
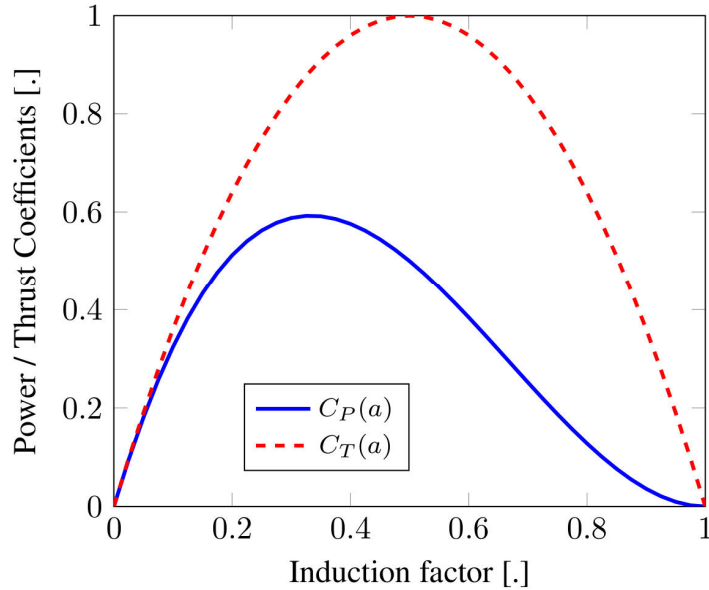
Figure 3: Variation of C_P and C_T with induction factor

1.2.2 Wake rotation

When the wind blows through the rotor, a rotation is observed as shown in Figure 4. Energy involved in this phenomenon is not taken into account with one-dimensional momentum theory. To improve the accuracy of performances predictions, one-dimensional momentum was supplemented by the angular momentum. The goal is to use the same logic as for the one-dimensional momentum theory but with angular momentum. Figure 5 shows the trajectory of an air particle through a wind turbine rotor. Thus, one finds that the rotational velocity of the particle is zero upstream of the rotor. The particle is rotated only at the rotor.

Figure 4: Wake rotation
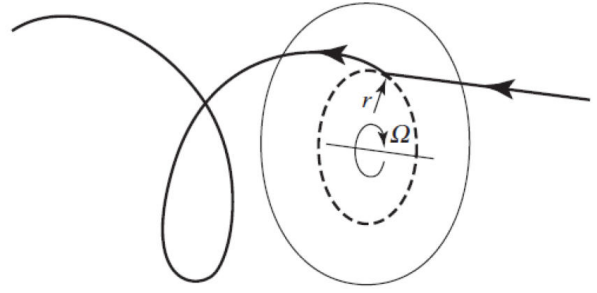
Figure 5: Trajectory of an air particle passing through the rotor disc [4]

Using the same notation as above, one can write the thrust force applied on a surface element $\mathrm{d}T$ due to angular momentum as:

$$\mathrm{d}T = (P_D^+ - P_D^-)\mathrm{d}A = \left(\rho\left(\Omega + \frac{1}{2}\omega\right)\omega r^2\right)2\pi r\mathrm{d}r, \tag{11}$$

where Ω and ω are, respectively, the rotation speed of the rotor and the rotation speed of the wind.

To simplify the relationship, the angular induction factor a' is introduced:

$$a' = \frac{\omega}{2\Omega}. \tag{12}$$

The thrust force applied on a surface element can be rewritten as:

$$\mathrm{d}T = 4a'(1+a')\frac{1}{2}\rho\Omega^2 r^2\,2\pi r\mathrm{d}r. \tag{13}$$

Equating the two relations for the thrust force, one arrives at:

$$\frac{a(1-a)}{a'(1+a')} = \frac{\Omega^2 r^2}{U_\infty^2} = \lambda_r^2, \tag{14}$$

where λ_r is the local tip speed ratio.

1.2.3 Torque

We now consider the torque recovered by the rotor. This torque is equal to the angular momentum multiplied by the radius:

$$\mathrm{d}Q = \mathrm{d}m(\omega r)(r) = (\rho U_D 2\pi r\,\mathrm{d}r)(\omega r)(r). \tag{15}$$

Using the same notations, one obtains:

$$\mathrm{d}Q = 4a'(1-a)\frac{1}{2}\rho U_D\Omega\,r^2 2\pi r\,\mathrm{d}r. \tag{16}$$

1.2.4 Conclusion

Finally, the momentum theory (one-dimensional and angular) leads to two relations. One for thrust force:

$$\mathrm{d}T = 4a(1-a)\rho\pi U_\infty^2 \, r\mathrm{d}r, \tag{17}$$

and one for torque:

$$\mathrm{d}Q = 4a'(1-a)\rho\pi U_\infty \Omega \, r^3 \mathrm{d}r. \tag{18}$$

1.3 Blade element theory

The momentum theory allows to calculate the thrust and the torque applied on the rotor disk as a function of the induction factor. The blade element theory allows to calculate the same loads (thrust and torque) recovered by a rotor composed of B blades. Figure 6 shows the distribution of the rotor elements.
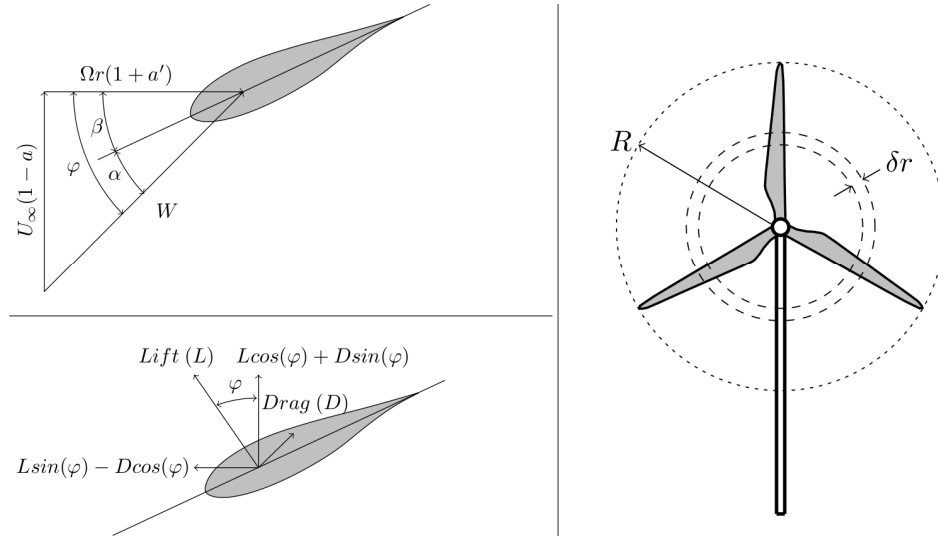
Figure 6: Scheme of a wind turbine annular element (right), velocity perceived by a blade element (top left) and forces acting on a blade element (bottom left)

Each element has a blade chord, c, and an element length, $\mathrm{d}r$. This element "sees" a relative velocity, W, composed of the velocity due to rotation, $\Omega r(1 + a)$, and the velocity due to the wind velocity, $U_\infty(1 - a)$. α, β and φ are respectively the attack angle, the twist angle and the angle between the relative velocity and the rotation plane of the element.

Finally, a lift force, a drag force and a moment are applied to the blade element in its base. Lift and drag forces lead to the normal and tangential forces to the rotation plane. These lift and drag forces are essentially function of the relative velocity (magnitude and direction). The twist angle is a geometrical constant, so that α and φ are related. φ can be determined by:

$$\tan\varphi = \frac{U_\infty(1-a)}{\Omega r(1+a')} = \frac{1}{\lambda_r}\frac{1-a}{1+a'}. \tag{19}$$

Then, one can calculate the attack angle α:

$$\alpha = \varphi - \beta. \tag{20}$$

The blades are determined by their profile shapes, or airfoils, defined by polar curves representing the lift and drag coefficients (Figure 7). For wind turbines, these curves are function of the attack angle and ideally the Reynolds number ($Re = \rho U c/\mu$).
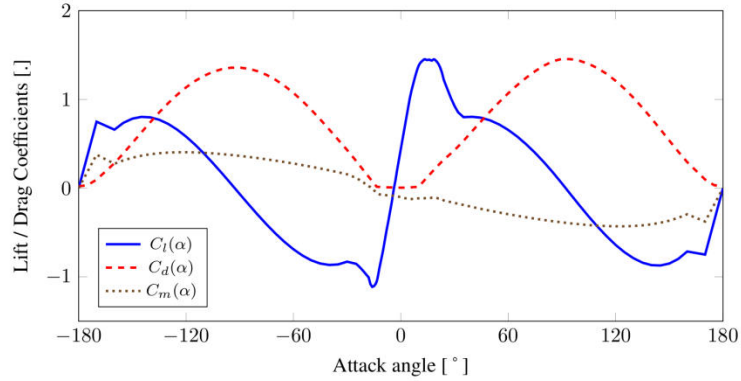
Figure 7: Variation of C_l, C_d and C_m with angle of attack (full range) for a NACA64-A17 airfoil

The relative velocity magnitude is obtained with:

$$W = \frac{U_\infty(1 - a)}{\sin \varphi}. \tag{21}$$

The lift (C_l) and drag (C_d) coefficients, and relative velocity magnitude allow to calculate the lift force, $\mathrm{d}F_L$, and the drag force, $\mathrm{d}F_D$:

$$\mathrm{d}F_L = C_l \frac{1}{2} \rho W^2 c \mathrm{d}r \tag{22}$$

$$\mathrm{d}F_D = C_d \frac{1}{2} \rho W^2 c \mathrm{d}r. \tag{23}$$

These forces allow to obtain normal and tangential forces at the rotation plane:

$$\mathrm{d}F_N^{blade} = \mathrm{d}F_L \cos \varphi + \mathrm{d}F_D \sin \varphi \tag{24}$$

$$\mathrm{d}F_T^{blade} = \mathrm{d}F_L \sin \varphi - \mathrm{d}F_D \cos \varphi. \tag{25}$$

1.4 BEM: combination of momentum and blade element theory

The two previous methods have identified expressions for the thrust force and the torque. The one-dimensional momentum and wake rotation theories lead to:

$$\mathrm{d}T = 4a(1 - a)\rho\pi U_D^2 \, r\mathrm{d}r \tag{26}$$

$$\mathrm{d}Q = 4a'(1 - a)\rho\pi U_D \Omega \, r^3\mathrm{d}r, \tag{27}$$

and the blade element theory leads to:

_____

$$dF_N = B.dF_N^{blade} = B\frac{1}{2}\rho W^2 (C_l \cos\varphi + C_d \sin\varphi)cdr \qquad (28)$$

$$dQ = B.r.dF_T^{blade} = B\frac{1}{2}\rho W^2 (C_l \sin\varphi - C_d \cos\varphi)crdr. \qquad (29)$$

Using the local solidity, σ':

$$\sigma' = \frac{Bc}{2\pi r}, \qquad (30)$$

the blade element theory leads to:

$$dF_N = \sigma'\pi\rho W^2 (C_l \cos\varphi + C_d \sin\varphi)rdr \qquad (31)$$

$$dQ = \sigma'\pi\rho \left(\frac{U_\infty(1-a)}{\sin\varphi}\right)^2 (C_l \sin\varphi - C_d \cos\varphi)r^2 dr. \qquad (32)$$

There are two unknowns in these equations: the induction factor, a, and the relative speed, W. But the relative speed is a function of the induction factor. To solve these equations, thrust forces are equalized. One obtains:

$$dT = dF_N \Leftrightarrow a(1-a) = \sigma'\frac{W^2}{U_D^2}(C_l \cos\varphi + C_d \sin\varphi) \qquad (33)$$

$$\Leftrightarrow a = 0.5\left(1 - \sqrt{1 - \sigma'\frac{W^2}{U_D^2}(C_l \cos\varphi + C_d \sin\varphi)}\right). \qquad (34)$$

However, it should be noted that if a changes then the relative velocity magnitude and its orientation also change. If the relative velocity changes, thus lift and drag coefficients also change. Calculation of the induction factor is done iteratively until a converged solution is obtained.

Similarly, one can equalize torque relationships to determine a':

$$dQ^{BE} = dQ^M \Leftrightarrow a' = \frac{\sigma'(1-a)(C_l \sin\varphi - C_d \cos\varphi)}{\lambda_r 4\sin^2\varphi}. \qquad (35)$$

1.5 Turbulent wake state and yawed actuator disk

1.5.1 Turbulent wake state

When the induction factor increases, there is a significant gap between the measured thrust force and the one predicted by BEM as shown in Figure 8. To take into account this phenomenon, empirical laws have been proposed. The principle is the use of an empirical law to calculate the induction factor.

One can use a Glauert-modified relationship [5]:

$$a = \frac{18 \times loss - 20 - 3\sqrt{C_T(50 - 36 \times loss) + 12 \times loss(3 \times loss - 4)}}{36 \times loss - 50}, \qquad (36)$$

where $loss$ is the hub and/or tip loss and

$$C_T = \frac{8}{9} + \left(4 \times loss - \frac{40}{9}\right)a + \left(\frac{50}{9} - 4 \times loss\right)a^2. \qquad (37)$$

This law is only used if the thrust coefficient C_T is higher than $0.96 \times loss$.
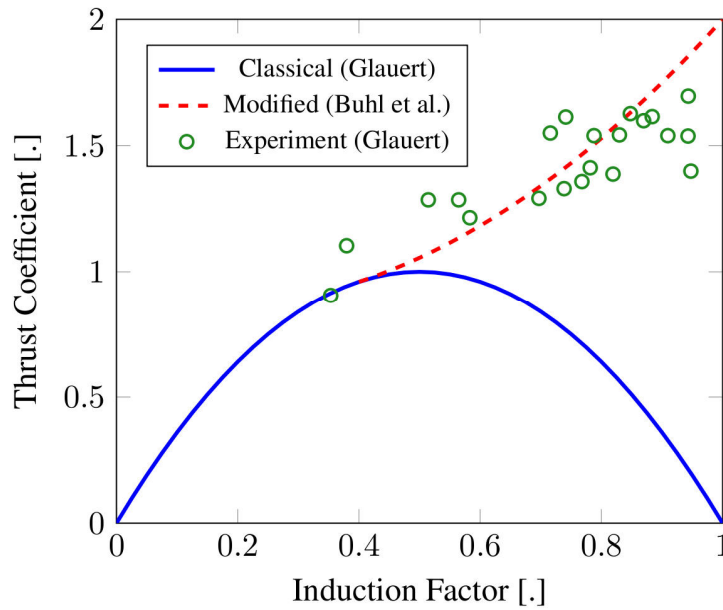
Figure 8: Comparison between thrust coefficients measured and predicted by BEM ($loss = 1$)

1.5.2 Wind and wind turbine misalignement

However, relation (37), that is commonly used, is not valid for the case of a yawed rotor. Relation (10), initial relation without turbulent wake state, is neither valid in this case. According to Madsen et al. [6], the relation derived by Stepniewski & Keys should be used for low values of the induction factor a ($a < \beta$) with $\beta \approx 0.35$ and γ the rotor misalignment angle:

$$C_T = loss \times 4a\sqrt{1 + a^2 - a \times 2\cos(\gamma)}.$$
(38)

At high loadings ($a > \beta$), the correction derived by Ning et al. [7] is used, with $C_{T,M}$ the thrust coefficient given by relation (37) :

$$\frac{C_T}{loss} = k_0 + k_1 a + k_2 a^2,$$

$$f_0 = C_{T,M} \; with \; a = \beta$$

$$f'_0 = \frac{dC_{T,M}}{da} \; with \; a = \beta$$

$$f_1 = p_{y1}\cos(\gamma)^{p_{y2}}$$
(39)

$$k_2 = \frac{f_1 - f_0 - f'_0(1 - \beta)}{(1 - \beta)^2}$$

$$k_1 = f'_0 - 2k_2\beta$$

$$k_0 = f_1 - k_1 - k_2$$

The two constant parameters take the default values $p_{y1} = 2$ and $p_{y1} = 0$.

1.5.3 Axial induction

Since in our implementation we need to get the axial induction factor knowing the thrust coefficient (see section (1.4)), the above expressions need to be inverted. Rather than using costly root-finding methods directly in the code, equation (39) has been first inversed using a Brent algorithm, and the results have been fitted using high order coefficients, given in appendix. This polynomial approximation is valid for thrust coefficients below $C_T = 1.75$. For higher thrust coefficients, the model automatically switches to a root-finding algorithm to determine the axial induction factor from the thrust coefficient.

1.6 Blade Element Momentum ad (BEAMad)

In this model, the equations are the same as for the BEM model. The only difference is the treatment of the velocity normal to the rotor. In BEM, the induction factor is applied to all velocities normal to the rotor. In BEMad, the induction factor is applied only to wind velocity normal to the rotor (see section 1.3). Thus, the induction factor is not applied for the velocity induced by the translation of the blade. It first intended to filter out the blade vibration velocities, which can be large, but this theory applies as well to floater motions while considering floating wind turbines. With this model, the relative wind created by these movements is not weighted by the induction factor. It would be preferable to replace this procedure by a low pass filter on all the velocities normal to the rotor.

1.7 Cutoffs

Under certain conditions, it might be useful to define reference tip speed ratio (TSR) values, TSR_{cutoff}, below and above which the induction factors computed by the BEM theory are set to zero. In *AeroDeeP*, the user can give these TSR_{cutoff} values as an input. In order to avoid non-smooth variations in aerodynamic loadings, which could have a negative impact on the aero-elastic coupling, a smoothing function is used to generate a transition between the cutoff regions and the BEM region, in the range of $TSR_{cutoff} - 0.5 < TSR < TSR_{cutoff}$, or $0 < TSR < TSR_{cutoff}$ in case $TSR_{cutoff} < 0.5$. This transition is performed using a linear interpolation between the induction factors computed with the BEM model and their values below the cutoff.

2 Secondary effects

The models presented above are used to estimate the energy converted by a system under optimal production conditions. In order to approach reality, additional corrections can be used.

2.1 Tip and hub loss

In BEM, it is assumed that blade element behavior is the same for an element in the center of the blade as for an element at the tip or at the root of the blade. But, in reality, losses are observed at the tip of the blade and at the root due to the hub. To take into account this phenomenon, Prandtl [8] proposes to add a parameter F in the momentum equations. Therefore, thrust and torque equations become:

$$dT = F4a(1-a)\rho\pi U_D^2 r\,dr \tag{40}$$

$$dQ = F4a'(1-a)\rho\pi U_D \Omega r^3\,dr. \tag{41}$$

F is the product of two functions representing respectively losses at beginning and at the end of the blade:

$$F = \underbrace{\frac{2}{\pi}\cos^{-1}\left(\exp\left(-\frac{\frac{B}{2}\left(1-\frac{r}{R_{Blade}}\right)}{\frac{r}{R_{Blade}}\sin\varphi}\right)\right)}_{\text{Tip loss}} \times \underbrace{\frac{2}{\pi}\cos^{-1}\left(\exp\left(-\frac{\frac{B}{2}\left(\frac{r}{R_{Hub}}-1\right)}{\frac{r}{R_{Hub}}\sin\varphi}\right)\right)}_{\text{Hub loss}}, \tag{42}$$

where R_{Hub}, R_{Blade} and r are respectively the hub radius, the blade radius (ie. hub radius plus blade length) and the element radius (element position on rotor disk).

Figure 9 shows the distribution of the loss coefficient along the blade.
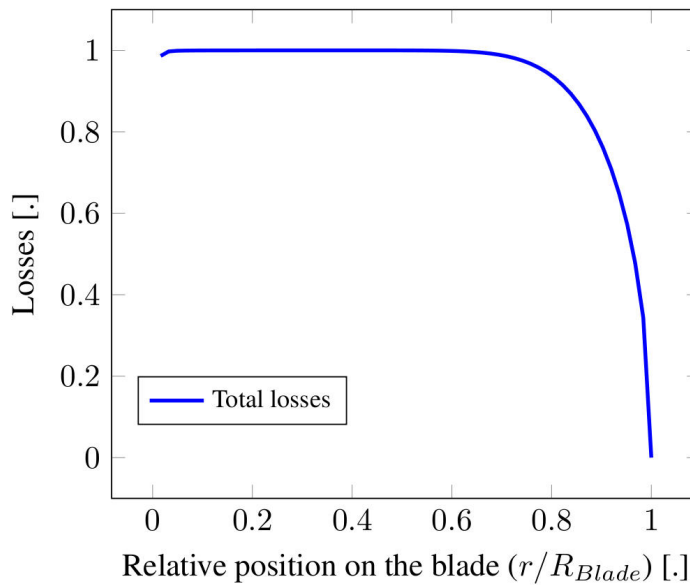

Figure 9: Loss coefficient as a function of the position on the blade ($\varphi = 9°$)

2.2 Tower effect

For horizontal axis wind turbines (HAWTs), as well as for vertical axis wind turbines (VAWTs), the tower may have an impact on the flow seen by the rotor. For HAWTs, the tower may have an impact upstream and downstream of itself. Upstream, the flow bypasses the tower, so there is an area where the flow is accelerated and another area where the flow is slowed. For upwind turbine, if the blade passes close enough to the tower, it can meet this area where the flow is disturbed by the tower [9]. For downwind wind turbines, the blades passes behind the tower and then passes into the tower wake. This phenomenon is known as "tower shadow" (Figure 10). Flow around a cylinder is a well-known subject. Many laws exist to calculate the flow behind a cylinder. Generally, these laws depend on the Reynolds number. In the case of wind turbines, it is assumed that the Reynolds number is large and the nature of the flow no longer Re-dependent.
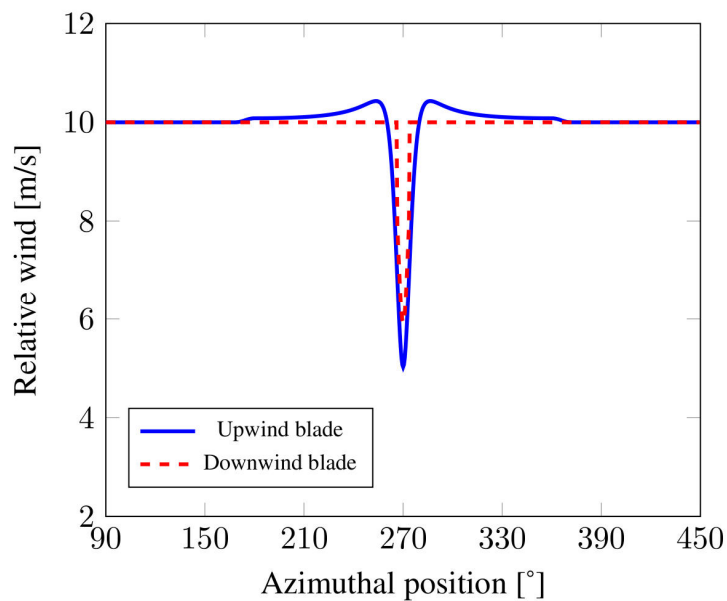
Figure 10: Tower shadow effect on the power during a full rotation of one-blade downwind and upwind the rotor

When the tower does not have a rotation speed (i.e. for HAWTs), this influence on the blade aerodynamics is modeled as in *AeroDyn* [3]. The tower's influence on the nearby dimensionless velocity field is based on:

$$U_{local} = (1 + u_t)U_\infty \tag{43}$$

$$V_{local} = (v_t)V_\infty,$$

$(1 + u_t)$ and v_t being the total dimensionless velocity deficit in the wake direction and perpendicular to the wake direction respectively. In order to compute those deficits, one computes separately the upstream deficit, due to potential effects, and the downstream deficit, due to the wake.

The upwind part is modeled as:

$$u_u = -\frac{R_{tower}^2 (x^2 - y^2)}{(x^2 + y^2)^2} + \frac{C_d}{2\pi} \frac{R_{tower} x}{x^2 + y^2} \tag{44}$$

$$v_u = -2\frac{R_{tower}^2 xy}{(x^2+y^2)^2} + \frac{C_d}{2\pi}\frac{R_{tower}\,y}{x^2+y^2},$$

R_{tower} being the tower radius at the considered elevation. The downwind part is modeled as:

$$\begin{cases} u_d = -\dfrac{C_d}{\sqrt{d}}\cos^2\left(\dfrac{\pi}{2}\dfrac{y}{R_{tower}\sqrt{d}}\right) & \text{if } |y| \le \sqrt{d} \\ u_d = 0 & \text{if } |y| > \sqrt{d} \end{cases} \tag{45}$$

where d is:

$$d = \sqrt{x^2+y^2}. \tag{46}$$

The distance can be altered to integrate the correction of Bak et al. : $x = x + b_{corr}R_{tower}$, with $b_{corr} = 0.1$ leading to the full potential flow solution.

Before merging the two models and in order to have a smooth transition between the upwind and downwind velocities above the tower, a vertical blending is applied for both upwind and downwind velocity deficits in the wake direction, as defined in [10]:

$$u_{u,d}^{blend} = f_v \times u_{u,d} = \begin{cases} u_{u,d} & \text{if } h_{tower} \\ u_{u,d} \times \dfrac{1}{2}\left(\cos\left(\dfrac{\pi(z-h_{tower})}{l_{blend}}\right)+1\right) & \text{if } h_{tower} < z \le h_{tower} + l_{blend}, \\ 0 & \text{if } z > h_{tower} + l_{blend} \end{cases} \tag{47}$$

l_{blend} being defined as the tower top diameter.

Then, another blending function is applied to merge the upwind and downwind model in the $x - y$ plane. The blending function writes:

$$f_a = \frac{1}{2}\left(\cos\left(\frac{\pi x}{r_{tower}}\right)+1\right) \tag{48}$$

and finally, one gets:

$$u_t = \begin{cases} u_u^{blend} & \text{if } x \le 0 \\ f_a u_u^{blend} + (1-f_a)u_d^{blend} & \text{if } 0 < x \le r_{tower} \\ u_d^{blend} & \text{if } x > r_{tower} \end{cases} \tag{49}$$

$$v_t = \begin{cases} v_u & \text{if } x \le 0 \\ f_a v_u & \text{if } 0 < x \le r_{tower} \\ 0 & \text{if } x > r_{tower} \end{cases} . \tag{50}$$

The effect of the vertical smoothing clearly appears on Figures 10 and 11. The transition between the zone of influence of the tower and the free stream is smooth and continuous.

The tower shadow model that includes the blending functions is referenced as the "IFPEN" model in the input file, while the standard tower shadow model is the default one ("Activated").
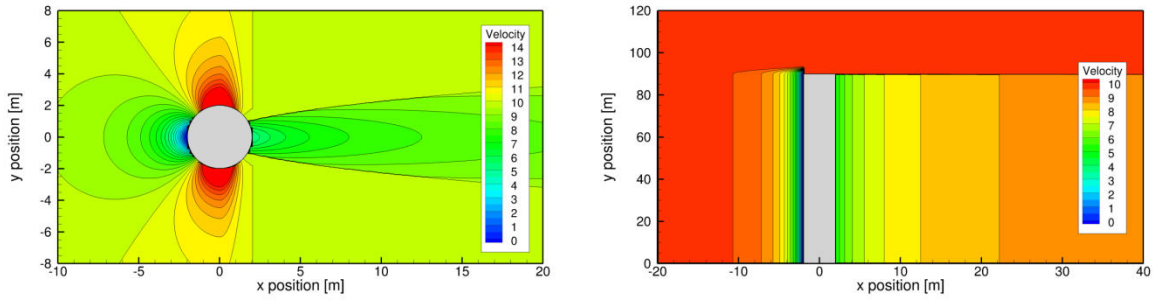
Figure 11: Velocity contours computed by the tower shadow model ($C_d = 0.75$) around a $r_{tower} = 2$m-tower, xy plane

2.3 Skewed Wake Correction

Skewed wake behind the rotor appears when wind turbines operate at an angle to the wind. However, BEM does not take into account this phenomenon. Several corrections have been introduced in order to improve results.

2.3.1 Glauert model

A first model is based on the work of Glauert [11] (see also [12]). The induction factors are modified as follows:

$$a = a_0 \left(1 + \frac{15\pi}{32} \frac{r}{R} \tan\frac{\chi}{2} \cos(\theta - \theta_1)\right),$$
(51)

with a_0 the original (uncorrected) induction factor. This correction depends on the radius R, the azimuth angle θ and the wake skew angle χ. This skew angle is calculated using the following formula: $\chi = \gamma(0.6a_t + 1)$, with a_t the rotor averaged induction factor and γ the misalignment angle (i.e. the relative angle between the rotor plane and the incoming wind vector). θ_1 is a phase angle.

2.3.2 IFPEN model

Another model developed by Blondel et al. [13] is also available. This model accounts for the presence of the root vortices (i.e. vortices that emanate from the root of the blade, that interact with the rotor plane). It can be viewed as a tradeoff between the Schepers model [14], that is based on a lot of constant parameters, and the simplistic Glauert model, that only accounts for the tip vortex. Using this model, the axial induction factor reads:

$$a = a_0 \left(1 + k_1 \frac{r}{R} \tan\frac{\chi}{2} \sin(\theta - \theta_1) + k_2 \left(1 - \frac{r}{R}\right) \tan\frac{\chi}{2} \sin(\theta - \theta_2)\right).$$
(52)

k_1, k_2 are the so-called "shape functions" and $\theta_1 = 0°$, $\theta_2 = 180°$, the phase angles. The shape functions take the following form (with $A_1 = 0.35$ a constant parameter, and r_{hub} the hub radius):

$$k_1 = (1 - A_1) + A_1 \frac{r - r_{hub}}{R - r_{hub}},$$
(53)

$$k_2 = 1 - A_1 \frac{r - r_{hub}}{R - r_{hub}}.$$
(54)

2.4 Dynamic stall

One can talk about stall when the boundary layer flow around a blade is detached. This causes a significant increase in drag. In static cases, this phenomenon depends on the attack angle of the flow with the airfoil. For dynamic cases, when the attack angle is function of time, stall appears for different attack angles than static cases.

This phenomenon is directly visible in Figure 12 where the lift coefficient versus the attack ("incidence") angle is presented. The dotted curve represents the dynamic behavior and the solid curve represents the static behavior.
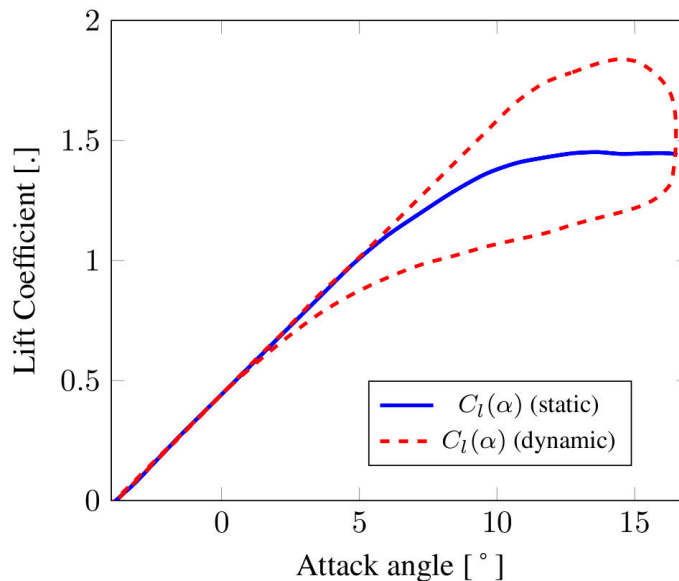
Figure 12: Lift coefficient C_l of a pitching airfoil: with and without dynamic stall

Note that the dynamic behavior introduces a hysteresis between detachment and reattachment of the boundary layer. Dynamic stall is a current subject of aeronautic research and several models exist. These models generally require parameters obtained through wind tunnel tests. Some models operate without these requirements such as the Boeing-Vertol model [15]. But they are less accurate. When using a dynamic stall model for coupled aero-elastic simulations, one should take care of the considered simulation time steps and the coupling with other phenomena, such as the tower shadow, which can cause fast and strong attack angle variations. Using a too large time step could thus lead to the instability of the models. As a recommendation, one should consider a time step small enough to have several points to discretize the blade passage in front of the tower.

2.4.1 Øye model

A first approach for modelling the dynamic stall phenomena is the one of Øye (see [16]), who suggested - if the angle of attack is below the full stall value - to simulate the stall phenomenon using a single ordinary differential equation representing the time lag of the separation point displacement. Øye defines a dynamic (f_d) and a static (f) attachment degree function, representing the position of the separation point on the suction side of the airfoil. The relation between the static and the dynamic functions simply writes:

$$\frac{df_d}{dt} = \frac{f - f_d}{\tau}, \tag{55}$$

τ being a time constant defined by Øye as $\tau = A_1\, c/V$, A_1 being a constant usually set to 4 by default, c the airfoil chord, and V the norm of the airfoil relative velocity. Once the static attachment function is determined, Equation 60 can be numerically integrated. To do so, one first needs to define the lift coefficient under fully attached ($C_{l,fa}$) and fully separated ($C_{l,fs}$) flow conditions. The actual lift coefficient, C_l, given by the airfoil polar, is nothing but a ponderation of those two coefficients and the attachment degree function. Thus, the function f can be found inverting the following relation:

$$C_l = f C_{l,fa} + (1 - f) C_{l,fs}. \tag{56}$$

The definition of the lift under fully attached flow conditions, $C_{l,fa}$, is based on the lift curve slope around α_0:

$$C_{l,fa} = \left.\frac{\partial C_l}{\partial \alpha}\right|_{\alpha_0} (\alpha - \alpha_0), \tag{57}$$

α_0 being the angle of attack where the lift value is zero.

The determination of the fully separated lift coefficient, $C_{l,fs}$, is a bit more tricky. In the current *AeroDeeP* implementation, we use a rather common approach (see [15], [17]), already introduced in [13], based on the Kirchhoff flow theory (Equation (58)) to determine a first attachment degree function value:

$$C_l \simeq \left(\frac{1 + \sqrt{f}}{2}\right)^2 C_{l,fa}. \tag{58}$$

Equation (58) is inverted, taking care of possible singularities, and then the value of f is used to determine the fully separated lift coefficient based on Equation (56). Finally, the dynamic lift coefficient computed using Equation (59), which is nothing but Equation (56) based on the dynamic attachment degree function:

$$C_{l,dyn} = f_d C_{l,fa}(\alpha) + (1 - f_d) C_{l,fs}(\alpha). \tag{59}$$

As shown in Equation (59), the Øye model only describes the dynamic lift evolution. Dynamic drag and moment coefficients are thus considered to be equal to their static counterparts.

2.4.2 Risø model

Another approach for simulating the dynamic stall phenomena has been proposed by Hansen et al. [17], and is based on a modified version of the Leishman-Beddoes model [18], which provides formulation for both the dynamic lift, drag, and moment coefficients. The most important assumptions in the model regarding the original Leishman-Beddoes formulation are the incompressible flow assumption effects (Mach number below 0.3) and the absence of leading edge separation (i.e. thick airfoil assumption). Only a very brief summary of the lift model will be given here. For a more complete description, the reader is referred to the original articles [18], [17]. The basic idea of the model is quite similar to the Øye model. An unsteady lift coefficient under attached flow conditions ($C_{l,fa}$) and an unsteady lift coefficient under fully separated flow conditions ($C_{l,fs}$) are computed, based on an effective angle of attack. This effective angle of attack aims at taking into account the downwash (change in flow direction) due to the presence of the near wake behind the airfoil. For the attached flow conditions and under the assumption of small amplitude motions of the airfoil, the Theodorsen theory is used to represent the effect of vortex shedding due to the wake, and leads to

the definition of two state variables, x_1 and x_2, representing the downwash times the relative velocity, which have to be solved for:

$$\dot{x}_i + \frac{2V}{c}\left(b_i + \frac{c\dot{V}}{2V^2}\right)x_i = b_i A_i \frac{2V}{c}\alpha, \tag{60}$$

$\dot{x}_i$ representing the time derivative of the scalar x_i, with $i = 1,2$. Using those two state variables, the effective angle of attack can be computed:

$$\alpha_e = \alpha(1 - A_1 - A_2) + x_1(t) + x_2(t). \tag{61}$$

Then, the unsteady lift under attached flow conditions writes:

$$C_{l,fa} = \left.\frac{\partial C_l}{\partial \alpha}\right|_{\alpha_0}(\alpha_e - \alpha_0) + \pi c\frac{\dot{\alpha}}{2V}. \tag{62}$$

For the lift under fully separated flow conditions ($C_{l,fs}$), the approach is identical to the one introduced in 2.4.1, based on Kirchhoff flow model, and thus will not be recalled here. Contrary to the Øye model, additional ODEs (ordinary differential equation) will now be introduced to model the dynamic trailing-edge separation. First, a time-lag between the lift and the airfoil pressure distribution is supposed, and is represented by a first order filter on the fully attached lift coefficient ($x_3(t) = C'_{l,fa}$):

$$\dot{x}_3 + T_p^{-1}x_3 = T_p^{-1}C_{l,fa}, \tag{63}$$

leading to the definition of a new angle of attack:

$$\alpha_f = C'_{l,fa} / \left(\left.\frac{\partial C_l}{\partial \alpha}\right|_{\alpha_0}\right) + \alpha_0, \tag{64}$$

and thus to a new attachment degree function, f', based on this new angle of attack, still computed using the approach introduced in 2.4.1. Then, an additional ODE arises due to the time-lag of the separation point position. Again, a first order filter is used to introduce an unsteady attachment degree function ($x_4 = f''$):

$$\dot{x}_4 + T_f^{-1}x_4 = T_f^{-1}f'(t). \tag{65}$$

Finally, the dynamic lift coefficient is computed:

$$C_{l,dyn} = \left.\frac{\partial C_l}{\partial \alpha}\right|_{\alpha_0}(\alpha_e - \alpha_0)f'' + C_{l,fs}(\alpha_e)(1 - f'') + \pi c\frac{\dot{\alpha}}{2V}. \tag{66}$$

Additionally to the lift model, a drag model and a moment model are proposed in [17], but will not be recalled here for the sake of brevity.

Finally, the Risø model for the lift coefficient can be written as a set of four ODEs:

$$\begin{aligned}
\dot{x}_1 + \frac{2V}{c}\left(b_1 + \frac{c\dot{V}}{2V^2}\right)x_1 &= b_1 A_1 \frac{2V}{c}\alpha \\
\dot{x}_2 + \frac{2V}{c}\left(b_2 + \frac{c\dot{V}}{2V^2}\right)x_2 &= b_2 A_2 \frac{2V}{c}\alpha \\
\dot{x}_3 + T_p^{-1}x_3 &= T_p^{-1}C_{l,fa} \\
\dot{x}_4 + T_f^{-1}x_4 &= T_f^{-1}f'(t)
\end{aligned} \tag{67}$$

T_p and T_f both represent time scales, and might be fitted on experiments. Recommended values are given in Table 1. Additional curve fitting constants A_1, A_2, b_1 and b_2 also have to be determined. Typical values are given in [17] (see also Table 1).

T_p	T_f	A_1	A_2	b_1	b_2
1.7	6.0	0.165	0.335	0.0455	0.3000

Table 1: Recommended values for the Risø dynamic stall model constants

Direct integration of Equation 72 might lead to an unstable solution and high computational costs. Thus, as suggested in [17], an high order indicial formulation was preferred in the current *AeroDeeP* implementation.

2.4.3 Boeing-Vertol model (deprecated)

The Boeing-Vertol model [15] assumes a relationship between the static and dynamic stall angle to determine a dynamic angle of attack α_d in the entire range of α. The relationship is given as:

$$\alpha_d - \alpha = A_1 \sqrt{\frac{c|\dot\alpha|}{2V}} \frac{\dot\alpha}{|\dot\alpha|}, \tag{68}$$

where $A_1 = 0.87$ in [11]. Now $C_{l,d}$ is determined as:

$$C_{l,d} = C_l(0) + \frac{C_l(\alpha_d) - C_l(0)}{\alpha_d} \alpha. \tag{69}$$

The theory of the model is illustrated in Figure 13, where the static and dynamic lift curves are plotted as dashed and bold full lines, respectively. Consider an angle of attack α_1 in the linear domain during increasing α, hence $\alpha > 0$. Using above equation gives a related dynamic angle of attack α_{d1} which is less than α_1. Now, $c_l(\alpha_{d1})$ is indicated by circles, the slope of the line going from $c_l(\alpha_d)$ is evaluated, giving the fraction in the above equation. Finally, $c_{l,d}$ illustrated by circles is determined from the above equation. In the linear domain, the slope determined at α_d is equal to the slope of the static lift, thus, no distinction can be made between the static and dynamic lift curve. Now, consider an angle of attack α_2 in the stall regime. Again, the corresponding dynamic angle of attack α_{d2} is found from the above equation. Then, the slope determined at α_d is less than that of the fully attached region, making $c_{l,d}(\alpha_2)$ less than that of a linear growing lift. This creates a dynamic stall cyclic behavior as indicated in Figure 13. For $\alpha = 0$, it is easily seen that the combination of equations above generates the static lift, i.e. the dynamic curve crosses the static curve for $\alpha = 0$.
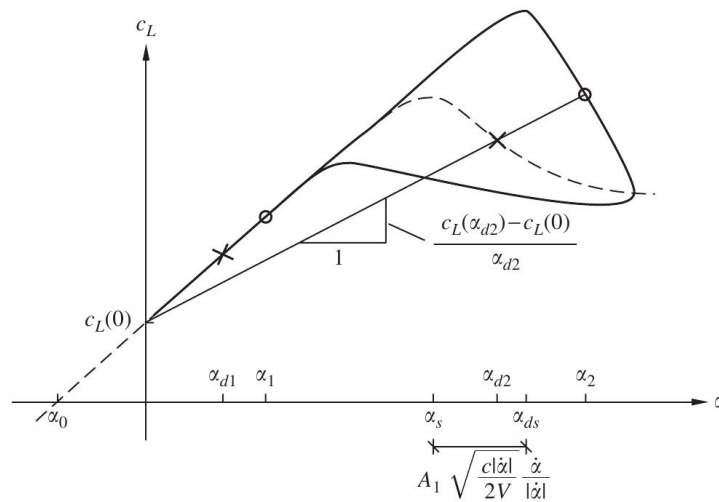
Figure 13: Illustration of the Boeing-Vertol model. − −, Static lift. −, Dynamic lift. X, Quasi-static angle of attack. ̊, Dynamic angle of attack, from [15]

2.4.4 Airfoil tables interpolation

AeroDeeP is able to handle the Reynolds dependency for the input tables. Cubic spline interpolations are performed between the angles of attack, and then linear interpolation are performed between the Reynolds numbers.

2.5 Stall delay (3D effects)

The accuracy of Blade Element Momentum methods is very sensitive to the input airfoils data (lift, drag and moment coefficients as function of the angle of attack). When available, those data come from experimental measurements. However, those measurements are performed in non-rotating conditions with two-dimensional airfoils (or blades with constant shape airfoils). Using those data for wind turbines calculations may result in inaccuracies: rotational and three-dimensional effects have to be taken into account. To achieve this, several models have been proposed in the literature. Figure 14 shows the effect of such models on a rotating turbine blade (experimental data extracted from [19]).
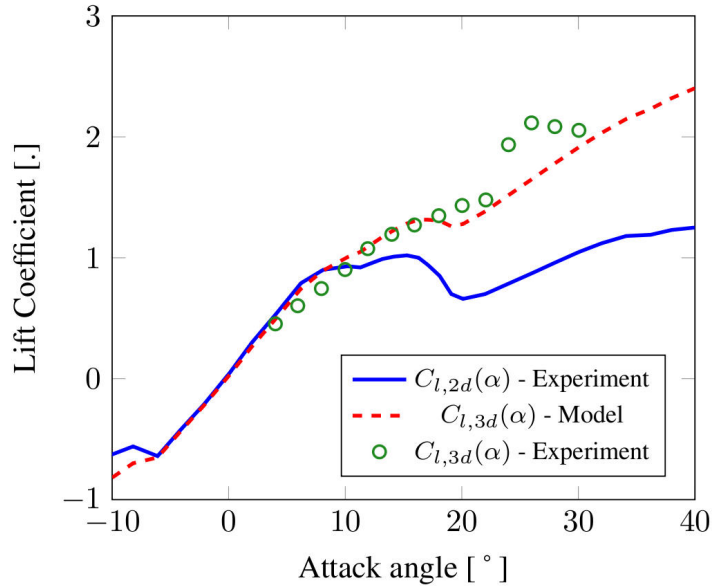
Figure 14: Influence of three dimensional effects and rotation on C_l

2.5.1 Snel model

Based on experimental measurements, the model of Snel (originally presented in [12]) including local speed ratio dependency (see [19] for a review) corrects the lift coefficient for those effects:

$$C_{l,3d} = C_{l,2d} + k_{Snel} \frac{\lambda_s}{1.0 + \lambda_s} \left(\frac{c}{r}\right)^2 \left(C_{l,pot} - C_{l,2d}\right) \tag{70}$$

$$C_{l,pot} = \left.\frac{\partial C_l}{\partial \alpha}\right|_{\alpha_0} \sin(\alpha - \alpha_0). \tag{71}$$

The constant of the model is, by default: $k_{Snel} = 3.1$.

2.5.2 Dumitrescu model

Alternatively, the model of Dumitrescu et al. [20] can be used. This model has a stronger impact on the lift coefficient, and a good agreement with experimental measurements has been obtained in previous studies [21].

$$c_{l,3D} = c_{l,2D} + \left[1 - exp\left(-\frac{\gamma}{\frac{r}{c} - 1}\right)\right] \Delta c_{l,1} \tag{72}$$

$$\Delta c_{l,1} = 2\pi \sin(\alpha_1 - \alpha_0) - c_{l,2D}(\alpha)$$

Based on Dumitrescu et al. suggestion, we will use the following constant parameter: $\gamma = 1.25$. Furthermore, a limiter is applied in equation (72) in order to avoid the divergence of the solution:

$$c_{l,3D} = c_{l,2D} + \left[1 - exp\left(-\frac{\gamma}{\max\left(1 \times 10^{-5}, \frac{r}{c} - 1\right)}\right)\right]\Delta c_{l,1} \tag{73}$$

2.5.3 Additional Lindenburg tip correction

Lindenburg [22] suggested an additional correction that diminishes the lift coefficient near the tip of the blade. This correction should be applied outboard, above a relative radius of 0.8. This model is justified by the impact of the radial flow, present at mid-span due to the rotational effects. This radial flow tends, according to Lindenburg, to reduce the negative pressure on the suction side of the airfoils, compared to the non-rotating case. Based on the UAE Phase VI experimental data, Lindenburg derived the following empirical law:

$$c_{l,3D,tip} = c_{l,2D} - \left(\frac{\Omega r}{U_{rel}}\right).e^{-2AR_{out}}.(c_{l,pot} - c_{l,2D})\frac{c_{l,2D}}{c_{l,pot}} \tag{74}$$

In practice, a constant "outboard aspect ratio" $AR_{out} = 2.0$ has been used in our implementation.

2.6 Dynamic Inflow

In the classical formulation of the Blade Element Momentum theory, an instantaneous equilibrium is supposed between the wind turbine and its wake. However, when a change occurs in the turbine operating conditions (i.e. a variation in wind speed or operating angle), a lag is observed before a new equilibrium state is reached. This lag is due to the viscous nature of the wind turbine wake, and can be modeled using an appropriate model.

In *AeroDeeP* , the choice has been made to use the two-differential equation model of Øye, where W represents the induced velocities, $a \times U$:

$$W_{int} + \tau_1 \frac{dW_{int}}{dt} = W_{qs} + k\tau_1 \frac{dW_{qs}}{dt} \tag{75}$$

$$W_{dyn} + \tau_2 \frac{dW_{dyn}}{dt} = W_{int} \tag{76}$$

$$\tau_1 = \frac{k_{1\tau1}}{1 - k_{2\tau1}a} \frac{R}{V_0} \tag{77}$$

$$\tau_2 = \left(k_{1\tau2} - k_{2\tau2}\left(\frac{r}{R}\right)^2\right)\tau_1. \tag{78}$$

The time constants, τ_1 and τ_2, have been determined from potential flow calculations.

The resolution method suggested by Hansen [23] has been used:

$$H = W_{qs} + k\tau_1 \frac{W_{qs}^i - W_{qs}^{i-1}}{\Delta t} \tag{79}$$

$$W_{int}^i = H + \left(W_{int}^{i-1} - H\right)e^{-\Delta t/\tau_1} \tag{80}$$

$$W_{dyn}^i = W_{int}^i + \left(W_{dyn}^{i-1} - W_{int}^i\right)e^{-\Delta t/\tau_2}. \tag{81}$$

The model constants take the following default value: $k_{1\tau 1} = 1.1$, $k_{2\tau 1} = 1.3$, $k_{1\tau 2} = 0.39$, $k_{2\tau 2} = 0.26$, $k = 0.6$.

The effect of the model is represented on Figure 15. An instantaneous pitch step is applied on the turbine blades at time $t = 5$ s. A damping appears with the dynamic inflow model, between $t = 5$ s and $t = 10$ s. The turbine reaches a new equilibrium state at time $t = 10$ s.
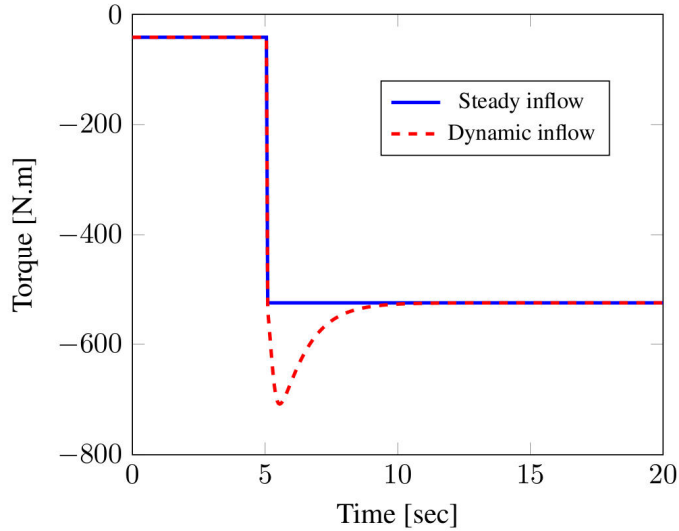
Figure 15: Dynamic inflow effect on rotor torque during a pitching step

In *AeroDeeP*, the induction factor a that is considered in the dynamic inflow model is not corrected for the "Skewed-wake" effect (see Section 2.3). However, it includes the advancing/retreating velocity effects due to the relative motion of the blade in case of rotor misalignment (i.e. misalignment with respect to the incoming wind). Thus, a cannot be considered as a purely "axial" induction factor, since it integrates some effects due the rotor plane misalignment.

3   Reference frames and relative velocities

The reference frames relative to the blade element and the hub used in *AeroDeeP* are depicted on Figure 16. These reference frames are directly provided by DeepLinesWind™.

Figure 16: Reference frames used for the calculation of the relative velocities, view from top

The position, orientation, and velocity matrices of the elements and components are defined in the global frame of reference. Then, we use matrix transformations to be able to write a given vector in a specific coordinate system to another reference system. As an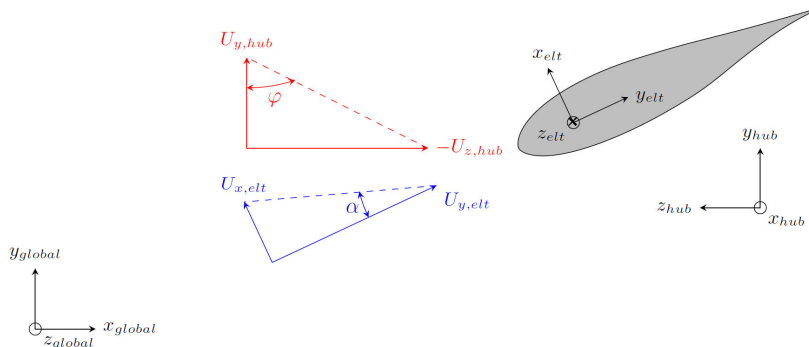 example, if one needs to express the vector coordinates of element relative velocities belonging to the element reference frame into the hub reference frame, two matrix vector products have to be performed:

$$\vec{U}_{relative,global} = M_{elt \to global} \, \vec{U}_{relative,element} \tag{82}$$

$$\vec{U}_{relative,hub} = M_{global \to hub} \, \vec{U}_{relative,global}. \tag{83}$$

The matrix used to transform from the element system to the global system, $M_{elt \to global}$, is simply the transpose of the matrix to transform from the global system to the element system.

Using the reference frames and relative velocities projections defined in Figure 16, the attack angle simply become:

$$\alpha = \operatorname{atan}\left(\frac{U_{x,elt}}{U_{y,elt}}\right), \tag{84}$$

the relative velocity simply being the difference between the wind velocity and the element velocity, altered by the induction factors.

In *AeroDeeP*, three BEM models have been implemented (see [24]):

- BladeElementMomentum
- BEMad

These two models differ in the way the relative velocities are computed. In the first model, the global element velocity is taken into account during the iterative procedure. In the second, the element structural velocity is excluded. In mathematical form, the first model writes, in the hub reference frame:

$$\begin{cases} U_{rel,x} = (1 + a')U_{wind,x} - (1 + a')U_{element,x} \\ U_{rel,y} = (1 + a')U_{wind,y} - (1 + a')U_{element,y} \\ U_{rel,z} = (1 - a)U_{wind,z} - (1 - a)U_{element,z} \end{cases} \tag{85}$$

whereas the second writes:

$$\begin{cases} U_{rel,x} = (1 + a')U_{wind,x} - (1 + a')U_{element,x} \\ U_{rel,y} = (1 + a')U_{wind,y} - (1 + a')U_{element,y} \\ U_{rel,z} = (1 - a)U_{wind,z} - \qquad\qquad U_{element,z} \end{cases} \tag{86}$$

Both models use the transformation matrices as defined above. Those two models have been implemented to give some freedom to the user, but we recommend the use of the first one, namely "BladeElementMomentum".

4 Global iterative procedure

In order to compute the forces and torques at any blade element, the following algorithm is applied:

Algorithm 1: Global BEM algorithm in *AeroDeeP*

Data: Position, orientation, and velocities of the blade element and turbine components.

Wind velocity in the global frame of reference.

Airfoils properties.

Values of induction factors (static and dynamic) from the last iteration.

Angles of attack from the last iteration.

Result: induction factors and inflow angle

initialization with values from the last iteration;

correct the wind velocity with the tower shadow model (§2.2);

while ($\Delta\alpha$ and $\Delta\varphi > tol$) **do**

    calculate the current element relative velocity;

    evaluate the current angle of attack α based on the relative velocity vector;

    evaluate the inflow angle φ based on the relative velocity vector in the hub reference frame ;

    determine the Reynolds number and look for corresponding lift, drag and moment coefficients in the airfoils tables;

    eventually, correct the computed coefficients for three dimensional/rotation effects (§2.5) and/or dynamic stall (§2.4);

    compute the tip and hub loss factors (§2.1) and determine the thrust coefficient CT (§1.5);

    compute induction factor a using the polynomial fit (88);

    compute the tangential induction factor a' (35);

    relax the new value of the induction factor for the next iteration;

end

correct the induction factor for dynamic inflow (§2.6);

correct the induction factor for skewed wake a_{skew} (§2.3);

correct the induction factor for dynamic stall (§2.4) and/or three dimensional/rotation effects (§2.5);

As shown in Algorithm 1, the root finding algorithm is based on a simple-fixed point algorithm, that uses a relaxation factor to prevent from divergence. After each iteration, the new value of the induction factor is relaxed using:

$$a_{new} = a_{old} + 0.5 \times (a_{new} - a_{old}) \tag{87}$$

_____

where a_{new} is the value of the last computed induction factor (the relaxation is not applied on the tangential induction factor).

5 Recommended options

The sample XML file below recapitulates the recommended values for the models described above.

```xml
<?xml version="1.0" encoding="utf-8"?>

<AERODEEP DTDRevision="v1.1"
          xsi:noNamespaceSchemaLocation="aerodeep_v21.xsd"
          xmlns:xsi="http://www.w3.org/2001/XMLSchema-instance">

  <MODEL name="BladeElementMomentum" min_tsr="1." max_tsr="30."/>

  <SECONDARY_EFFECT

                    tipLoss         = "Prandtl"
                    hubLoss         = "Prandtl"
                    tower_shadow    = "Activated"
                    stall_model     = "Oye"
                    skewed_model    = "IFPEN"
                    dynamic_inflow  = "Activated"
                    threeD_effects  = "None" />



  <FLUID density="1.225" viscosity="1.81206e-5"/>

</AERODEEP>
```

References

[1] J. Manwell, J. McGowan et A. Rogers, Wind Energy Explained: Theory, Design and Application, Wiley, 2010.

[2] E. Bossanyi et D. Quarton, «GH Bladed - Theory Manual,» Garrad Hassan and Partners Limited, 2003.

[3] P. Moriarty et A. Hansen, «AeroDyn Theory Manual,» 2005.

[4] T. Burton, D. Sharpe, N. Jenkins et E. Bossanyi, Wind Energy Handbook, John Wiley & Sons, second edition, 2001.

[5] L. Buhl, «A new empirical relationship between thrust coefficient and induction factor for the turbulent windmill state,» Technical report nrel/tp-500-36834, National Renewable Energy Laboratory, 2005.

[6] H. A. Madsen, T. J. Larsen, G. R. Pirrung, L. Ang et F. Zahle, «Implementation of the blade element momentum model on a polar grid and its aeroelastic load impact,» *Wind Energy Science,* vol. 5, n° %11, pp. 1-27, 2020.

[7] S. Ning, G. Hayman, R. Damiani et J. Jonkman, «Development and Validation of a New Blade Element Momentum Skewed-Wake Model within AeroDyn (preprint),» *AIAA Science and Technology Forum and Exposition,* 2015.

[8] L. Prandtl, «Schraubenpropeller mit geringstem energieverlust (zusatz zu a. betz),» pp. 93-197, 1919.

[9] P. Leconte et M. Rapin, «Machines aéodynamiques et compresseurs,» *Techniques de l'Ingénieur,* 2014.

[10] C. Crawford, «Advanced Engineering Models for Wind Turbines with Application to the Design of a Coning Rotor Concept (PhD thesis),» Trinity College - Department of Engineering, 2006.

[11] H. Glauert, «A General Theory of the Autogyro,» Reports and memoranda. H.M. Stationery Office, 1928.

[12] H. Snel, R. Houwink et J. Bosschers, «Sectional Prediction of Lift Coefficients on Rotating Wind Turbine Blades in Stall,» ECN / C: ECN. Netherlands Energy Research Foundation, 1994.

[13] F. Blondel, G. Ferrer, M. Cathelain et D. Teixeira, *Improving a BEM Yaw Model Based on NewMexico Experimental Data and Vortex/CFD Simulations,* CFM, 2017.

[14] J. G. Schepers, Engineering models in wind energy aerodynamics - Development, implementation and analysis using dedicated aerodynamic measurements, 2012.

[15] J. Larsen, S. Nielsen et S. Krenk, «Dynamic stall model for wind turbine airfoils,» *Journal of Fluids and Structures,23:959–982,* 2007.

[16] S. Øye, «Dynamic Stall Simulated as Time Lag of Separation,» Technical report, Technical University of Denmark, 1991.

[17] M. Hansen, M. Ganuaa et H. Madsen, «A Beddoes-Leishman type Dynamic Stall Model in State-Space and Indicial Formulations,» Technical report risø -r-1354(en), Risø National Laboratory, 2004.

[18] J. Leishman et T. Beddoes, «A generalised model for airfoil unsteady aerodynamic behaviour and dynamic stall using the indicial method,» *42nd. Annual Forum of the American Helicopter Society,* 1986.

[19] C. Bak, J. Johansen and P. Andersen, "Three-dimensional corrections of airfoil characteristics based on pressure distributions (paper and poster)," *European Wind Energy Association (EWEA),* 2006.

[20] H. Dumitrescu, H. Cardos et A. Dumitrache, «Modelling of inboard stall delay due to rotation,» *The Science of Making Torque from Wind, Journal of Physics: Conference Series 75 (2007) 012022,* 2007.

[21] F. Blondel, Investigation of the stall delay phenomenon on horizontal wind turbine blades, R0440R-FBl/CBe-18.0167, IFPEN, 2018.

[22] C. Lindenburg, «Investigation Into Rotor Blade Aerodynamics, ECN-C-03-025,» 2003.

[23] M. Hansen, «Aerodynamics of Wind Turbines,» Earthscan, earthscan edition, 2008.

[24] F. Blondel, P. Bozonnet, G. Ferrer, T. Perdrizet et D. Teixeira, «Users guide to AeroDeeP,» Technical report, IFPEN, 2011.

[25] R. Damiani, «Algorithm outline of unsteady aerodynamics (AeroDyn) modules,» Technical report we-201103, RRD Engineering, 2011.

6 Appendix A: polynomial fit for the induction factor in yaw

$$k_0 = -0.03650954963023791 * \gamma^3 - 0.010406485510328307 * \gamma^2 \\ + 0.187634868194944400 * \gamma - 0.10198290016206948$$

$$k_1 = +0.17341954565890796 * \gamma^3 + -0.212320835590612500 * \gamma^2 \\ + -0.289705458143211100 * \gamma + 0.23260734280797385$$

$$k_2 = -0.14633132594729326 * \gamma^3 + 0.278786061555097550 * \gamma^2 \\ - 0.077968315317758760 * \gamma + 0.05781887310182215$$

$$k_3 = +0.05080156142660903 * \gamma^3 - 0.138488946370084700 * \gamma^2 \\ + 0.108708441059442810 * \gamma + 0.20769821396129032$$

$$k_4 = -0.003582100801873169 * \gamma^3 + 0.011323623595503348 * \gamma^2 \\ - 0.011479799674274819 * \gamma + 0.0050536334424277915$$

(88)

$$a = k_0 \left(\frac{C_T}{loss}\right)^4 + k_1 \left(\frac{C_T}{loss}\right)^3 + k_2 \left(\frac{C_T}{loss}\right)^2 + k_3 \frac{C_T}{loss} + k_4$$

Principia SAS
215 Voie Ariane, ZI Athelia 1
13705 La Ciotat
France
Tel: +33 442 98 11 80
Fax: +33 442 98 11
80

Principia SAS
Rue de la Noë
44000 Nantes
France
Tel: +33 240 14 50 14
Fax: +33 240 14 34 00

Principia North A/S
Gronlandsvej 10
DK-5700 Svendborg
Denmark
Tel: +45 62 228 228
Mob: +65 22 169 811

Principia Asia Sdn Bhd
Level 32 - Menara Binjai
No. 2 Jalan Binjai
50450 Kuala Lumpur
Malaysia
Tel: +60 321660 400

www.principia.fr
deeplines@principia.fr

Head Office
Principia SAS
215 Voie Ariane, ZI Athelia 1
13705 La Ciotat
France
Tel: +33 442 98 11 80
Fax: +33 442 98 11
80

Nantes
Principia SAS
Rue de la Noë
44000 Nantes
France
Tel: +33 240 14 50 14
Fax: +33 240 14 34 00

Denmark
Principia North A/S
Gronlandsvej 10
DK-5700 Svendborg
Denmark
Tel: +45 62 228 228
Mob: +65 22 169 811

Kuala Lumpur
Principia Asia Sdn Bhd
Level 32 - Menara Binjai
No. 2 Jalan Binjai
50450 Kuala Lumpur
Malaysia
Tel: +60 321660 400